Endothelin type B receptor promotes cofilin rod formation and dendritic loss in neurons by inducing oxidative stress and cofilin activation

Received for publication, August 15, 2018, and in revised form, June 25, 2019 Published, Papers in Press, June 27, 2019, DOI 10.1074/jbc.RA118.005155

Sze-Wah Tam[‡§1], Rui Feng[‡], Way Kwok-Wai Lau[§¶], Andrew Chi-Kin Law[§‖], Patrick Ka-Kit Yeung[‡], and Sookja Kim Chung[‡‡‡2]**

*From the [‡]School of Biomedical Sciences, [§]Department of Psychiatry, **State Key Laboratory of Pharmaceutical Biotechnology, and [‡‡]Research Center of Heart, Brain, Hormone and Healthy Aging, The University of Hong Kong, Hong Kong, China, the [¶]Department of Special Education and Counseling, The Education University of Hong Kong, Hong Kong, China, and the [‖]Department of Psychiatry, Royal College of Surgeons in Ireland at Perdana University, Selangor, Malaysia*

Edited by Paul E. Fraser

Endothelin-1 (ET-1) is a neuroactive peptide produced by neurons, reactive astrocytes, and endothelial cells in the brain. Elevated levels of ET-1 have been detected in the post-mortem brains of individuals with Alzheimer's disease (AD). We have previously demonstrated that overexpression of astrocytic ET-1 exacerbates memory deficits in aged mice or in APP$^{K670/M671}$ mutant mice. However, the effects of ET-1 on neuronal dysfunction remain elusive. ET-1 has been reported to mediate superoxide formation in the vascular system via NADPH oxidase (NOX) and to regulate the actin cytoskeleton of cancer cell lines via the cofilin pathway. Interestingly, oxidative stress and cofilin activation were both reported to mediate one of the AD histopathologies, cofilin rod formation in neurons. This raises the possibility that ET-1 mediates neurodegeneration via oxidative stress– or cofilin activation–driven cofilin rod formation. Here, we demonstrate that exposure to 100 nM ET-1 or to a selective ET type B receptor (ET_B) agonist (IRL1620) induces cofilin rod formation in dendrites of primary hippocampal neurons, accompanied by a loss of distal dendrites and a reduction in dendritic length. The 100 nM IRL1620 exposure induced superoxide formation and cofilin activation, which were abolished by pretreatment with a NOX inhibitor (5 μM VAS2870). Moreover, IRL1620-induced cofilin rod formation was partially abolished by pretreatment with a calcineurin inhibitor (100 nM FK506), which suppressed cofilin activation. In conclusion, our findings suggest a role for ET_B in neurodegeneration by promoting cofilin rod formation and dendritic loss via NOX-driven superoxide formation and cofilin activation.

Increased expression levels of ET-1[3] have been detected in the frontal, temporal, and occipital lobes of the post-mortem brains of AD patients, when compared with age-match controls, with a more significant impact noted in the neurons, reactive astrocytes, and cerebral vessel walls (1–3). *In vitro* studies showed that β-amyloid (Aβ)-treated neuroblastoma cell line and reactive astrocytes exhibited highly increased ET-1 expression and secretion (2, 4). Astrocyte reactivity was detected in the brains of AD patients and AD transgenic mice, 3xTg-AD or APP[V717I] mice (3, 5–7). These studies have supported an up-regulation of ET-1 level in AD brain. Our team previously found that overexpression of astrocytic ET-1 induced early onset of memory deficit and exacerbated the performance decline in the 18-month-old APP$^{K670/M671}$ mutant mice using the Morris water maze test.[4] The same study also demonstrated that overexpression of astrocytic ET-1 impaired the performance of the aged 18-month-old mice in the spatial reference memory task. These findings suggested that increased ET-1 level in the brain could mediate neurodegeneration in AD or during aging. Although it is known that neurons express two subtypes of ET-1 receptor, type A (ET_A) and type B (ET_B) (8), the effects of ET-1 on mediating dysfunction of mature neurons are still poorly known.

ET-1 has been reported to regulate oxidative stress production and actin cytoskeleton. ET_A and ET_B mediate superoxide production in the vascular tissues of hypertensive mice and a human umbilical vein endothelial cell line, respectively, via NOX (9, 10). In contrast, ET-1 modulates migration and morphological changes of a protoplasmic astrocyte cell line, primary polymorphonuclear leukocytes, a podocyte cell line, and cancer cell lines by regulating actin cytoskeleton (11–14). Previous studies suggested that ET-1 might regulate actin polymer-

This work was supported by a generous donation from the Henderson Warmth Foundation and Chow Tai Fook Charity Foundation for dementia research (to A. C.-K. L.), the Research Grants Council and the University Grants Council of Hong Kong on "Molecular Neuroscience: Basic Research and Drug Discovery" (Grant AoE/B-15/01), and University of Hong Kong matching funds for the State Key Laboratory of Pharmaceutical Biotechnology (to S. K. C.). The authors declare that they have no conflicts of interest with the contents of this article.

This article contains Figs. S1–S3.

[1] To whom correspondence may be addressed. Tel.: 852-39179184; E-mail: cathy_tsw@connect.hku.hk.

[2] To whom correspondence may be addressed: School of Biomedical Sciences, Faculty of Medicine, The University of Hong Kong, 21 Sassoon Rd., Pokfulam, Hong Kong, China. Tel.: 852-39179172; E-mail: skchung@hku.hk.

[3] The abbreviations used are: ET-1, endothelin-1; AD, Alzheimer's disease; Aβ, β-amyloid; DIV, day(s) *in vitro*; DHE, dihydroethidium; ET_A, endothelin type A receptor; ET_B, endothelin type B receptor; Eth, ethidium; LIMK, LIM domain kinase; NAC, *N*-acetylcysteine; NOX, NADPH oxidase; SSH-1L, Slingshot homolog 1; APP, amyloid precursor protein; Nle, norleucine; 1°, primary; 2°, secondary; 3°, tertiary; 4°, quaternary; NA, numerical aperture; TBST, Tris-buffered saline with Tween 20; p-cofilin, phosphorylated cofilin; HRP, horseradish peroxidase; ANOVA, analysis of variance; HSD, honestly significant difference.

[4] Please refer to pp. 76–82, Chapter 4, of Ref. 43.

ization by modulating the activity level of cofilin via Rho-associated protein kinase/LIM domain kinase (LIMK) pathway in an ovarian cancer cell line (14). Interestingly, both oxidative stress and cofilin dysregulation were proposed to induce cofilin rod formation in neurons; this is one of the histopathologies observed in the post-mortem brains of AD patients (15–17). Cofilin rod formation was also observed in Aβ-treated primary neurons and *ex vivo* hippocampal slices (18). *In vitro* studies have shown that cofilin rod formation blocked intracellular trafficking and induced loss of synapses in distal neurites (16). In short, these results raised the hypothesis that ET-1 might mediate neuropathology via cofilin rod formation, which could be induced by NOX-mediated oxidative stress or cofilin dysregulation. Here, we demonstrate a novel neurodegenerative role of ET_B in mediating cofilin rod formation and loss of distal dendrites in primary hippocampal neurons via NOX-mediated superoxide production and dysregulated cofilin activation.

Results

Endothelin type B receptor mediates cofilin rod formation in dendrites of hippocampal neurons

Based on the previous *in vitro* studies (19, 20), relatively high concentrations, *i.e.* 1, 10, and 100 nM, of ET-1 were used to mimic the pathologically high level of ET-1 in the brain. Treatment time of 20 or 24 h is commonly used for demonstrating the effect of Aβ or proinflammatory cytokines on cofilin rod formation in neurons (18, 21). Therefore, we first examined the effect of 24-h treatment of 1, 10, or 100 nM ET-1 on cofilin rod formation in 14-day *in vitro* (DIV) primary hippocampal neurons. The 10 or 100 nM ET-1 treatment significantly increased the percentage of neurons with cofilin rods (Fig. 1, *A* and *B*). Further analysis showed that the average number of cofilin rods per neuron increased with increasing concentration of ET-1 (Fig. 1*C*). Thus, the highest concentration, 100 nM, of ET-1 was used in the following experiments. The time course and subcellular localization of ET-1–induced cofilin rod formation were further examined. The 100 nM ET-1 treatment significantly increased the percentage of neurons with cofilin rods and average number of cofilin rods per neuron after 1-, 2-, 4-, 8-, 16-, and 24-h treatment (Fig. 1, *D* and *E*). Besides, compared with the neurons treated with vehicle for 2, 4, 8, or 16 h, the neurons treated with vehicle for 24 h showed a significantly lower percentage of neurons with cofilin rods and a lesser number of cofilin rods per neuron (Fig. 1, *D* and *E*). These findings suggested that the spontaneously formed cofilin rods, which could have resulted from the stress induced by medium replacement during drug treatment or from vehicle treatment, disintegrated after 24 h treatment. Thus, the 24-h treatment time was used in the following experiments. Moreover, the triple immunofluorescence staining of cofilin, MAP2, and tau showed that ET-1–induced cofilin rods were located distally to the MAP2-positive dendrites (Fig. 1*F*).

Knowing that ET-1 could induce cofilin rod formation, we wondered which ET receptor subtype mediated this effect. A pharmacological approach was used to selectively block ET_A or ET_B using a selective ET_A antagonist, BQ123 (cyclo(D-Trp-D-Asp-Pro-D-Val-Leu)) and a selective ET_B antagonist, BQ788 (*N*-2,6-dimethylpiperidinocarbonyl-γ-MeLeu-Trp(COOMe)-Nle-ONa), which have been widely used for examining the roles of ET receptor *in vitro* and *in vivo*. Pretreatment with1 μM selective ET_B antagonist (BQ788), but not 1 μM selective ET_A antagonist (BQ123), abolished ET-1–induced cofilin rod formation (Fig. 2), indicating that ET_B activation mediates cofilin rod formation in hippocampal neurons.

Endothelin type B receptor agonist–induced cofilin rod formation is accompanied by the loss of distal dendrites and reduction in dendritic length

Previous studies proposed that cofilin rods could disrupt the microtubules in distal neurites (22). The fact that ET-1 induced cofilin rod formation in MAP2-positive dendrites via ET_B prompted us to find out whether ET_B activation–induced cofilin rods would affect the dendritic morphology. Hippocampal neurons were costained with cofilin and MAP2 after 24-h treatment with vehicle or 100 nM selective ET_B agonist (IRL1620). The MAP2-stained dendritic networks were then subjected to dendrite tracing. Neurons with cofilin rods (20 and 78.3% in vehicle group and IRL1620 treatment group, respectively) or without cofilin rods were both observed in the vehicle and IRL1620 treatment groups. Based on the presence of cofilin rods, neurons were subdivided into four groups: vehicle group with or without cofilin rods and IRL1620 treatment group with or without cofilin rods. Compared with the vehicle-treated neurons without cofilin rods, the IRL1620-treated neurons with cofilin rods had a significantly shorter maximum extension radius and lower number of intersections at 230–450 μm away from the center of the soma in Sholl analysis (Fig. 3, *B* and *C*). These results indicated that ET_B activation led to the loss of distal dendrites. Interestingly, in the IRL1620-treated neurons, most of the cofilin rods were located distally at 175–275 μm away from the center of the soma (Fig. 3*D*) which were proximal to and partly overlapping with the distance range of the neurons that showed a significantly lower number of intersections in Sholl analysis (Fig. 3*C*). Moreover, consistent with the reported effect of cofilin rods on disruption of microtubules, reduction in MAP2 intensity was observed around the cofilin rods in vehicle- or IRL1620-treated neurons. Further quantification revealed that MAP2 signals were significantly decreased at the proximal side of cofilin rods or between the cofilin rods in the IRL1620-treated neurons (Fig. 4). In short, these findings suggested that one of the possible mechanisms behind ET_B activation–induced loss of distal dendrite was the formation of distally located cofilin rods that could disrupt nearby microtubules.

Next, we examined how IRL1620 treatment could lead to the loss of distal dendrites. Cofilin rods were distributed in primary (1°) to quaternary (4°) dendrites of neurons treated with vehicle or IRL1620 (Fig. 5*D*). Compared with the vehicle-treated neurons without cofilin rods, the IRL1620-treated neurons with cofilin rods had significant reduction in the average length of 1°–4° dendrites (Fig. 5*A*) but had no significant difference in the number of branch points or Schoenen ramification index (Fig. 5, *B* and *C*). These findings suggested that the loss of distal

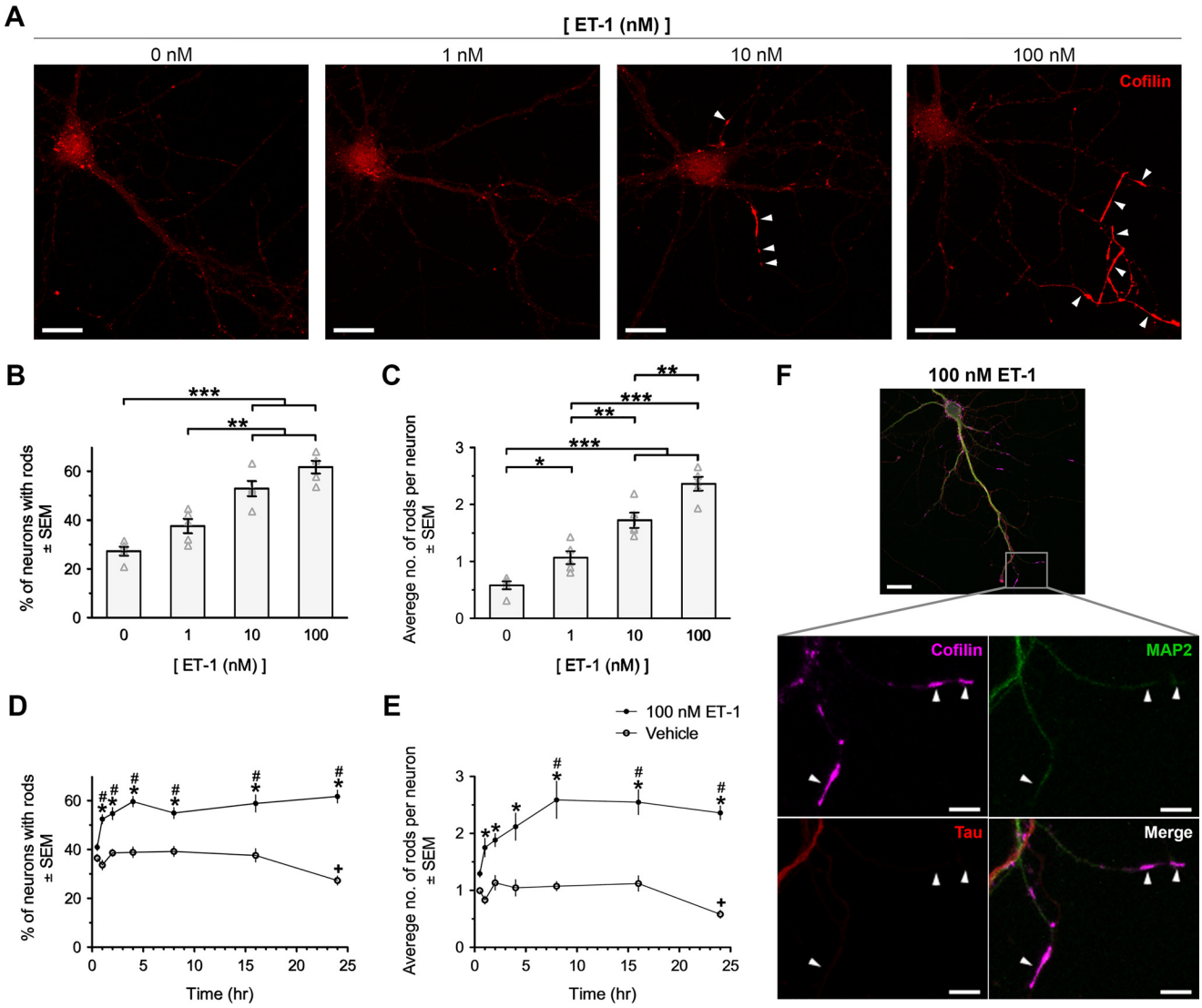

Figure 1. Endothelin-1 induced cofilin rod formation in MAP2-positive dendrites of primary hippocampal neurons. Primary hippocampal neurons were treated with ET-1 at 14 DIV. The vehicle group was treated with 0.005% (v/v) acetic acid. After treatment, neurons were fixed and stained for cofilin rod quantification. At least 200 neurons were observed for each treatment group per trial. With a total of five trials, at least 1000 neurons were observed for each treatment group. *A*, representative confocal images show the immunofluorescence staining of cofilin in neurons treated with 0, 1, 10 or 100 nM ET-1 for 24 h. *Arrowheads* indicate cofilin rods formed in the neurons treated with 10 or 100 nM ET-1. *B* and *C*, the percentage of neurons with cofilin rods and average number of cofilin rods per neuron after 24-h treatment with 0, 1, 10, or 100 nM ET-1. *, $p < 0.05$; **, $p < 0.01$; ***, $p < 0.001$, one-way ANOVA with Tukey HSD post hoc test. Data were obtained from five independent experiments ($n = 5$). *D* and *E*, the percentage of neurons with cofilin rods and average number of cofilin rods per neuron after 0.5-, 1-, 2-, 4-, 8-, 16-, or 24-h treatment with 100 nM ET-1. *, $p < 0.001$ *versus* corresponding vehicle group, two-way ANOVA with Bonferroni correction; #, $p < 0.05$ versus 0.5-h ET-1 treatment group; +, $p < 0.05$ *versus* 2-, 4-, 8-, and 16-h vehicle group, one-way ANOVA with Tukey HSD post hoc test. Data were obtained from five independent experiments ($n = 5$). *F*, representative confocal images show the triple immunofluorescence staining of cofilin (*magenta*), MAP2 (dendritic marker; *green*), and tau (axonal marker; *red*) in a neuron treated with 100 nM ET-1 for 24 h. ET-1–induced cofilin rods were located in the distal MAP2-positive dendrites. This result was obtained by analyzing a total of 51 cofilin rods from 20 neurons pooled from two independent trials. *Scale bars*, 20 μm (5 μm in *enlarged views* in *F*). *Error bars* represent S.E.

dendrites observed in IRL1620-treated neurons with cofilin rods was due to dendrite shortening instead of dendritic shrinkage. Interestingly, when comparing the vehicle- or IRL1620-treated neurons without cofilin rods, the IRL1620-treated neurons showed significant reduction in average length of 4° dendrites and a trend of reduction in the length of 2° and 3° dendrites ($p = 0.051$ and 0.076 for 2° and 3° dendrites, respectively). This result suggested that ET_B activation could induce shortening of 2°–4° dendrites without inducing cofilin rod formation. Therefore, these results demonstrate that ET_B activation leads to dendrite shortening regardless of the formation of cofilin rods.

Endothelin type B receptor mediates superoxide formation and cofilin rod formation via NADPH oxidase

A previous study reported that oxidation on cysteine residues of cofilin was essential for formation of intermolecular disulfide bonds and subsequent oligomerization of cofilin (15). We also found that cotreatment with antioxidant *N*-acetylcysteine (NAC) abolished ET-1– or IRL1620-induced cofilin rod formation (Fig. 6, *A* and *B*). Previously, Aβ oligomers or proinflammatory cytokines were shown to induce cofilin rod formation in neurons via NOX-driven oxidative stress (21). NOX predominantly contributes to the generation of superoxide (23). These results made us wonder whether ET_B activation also

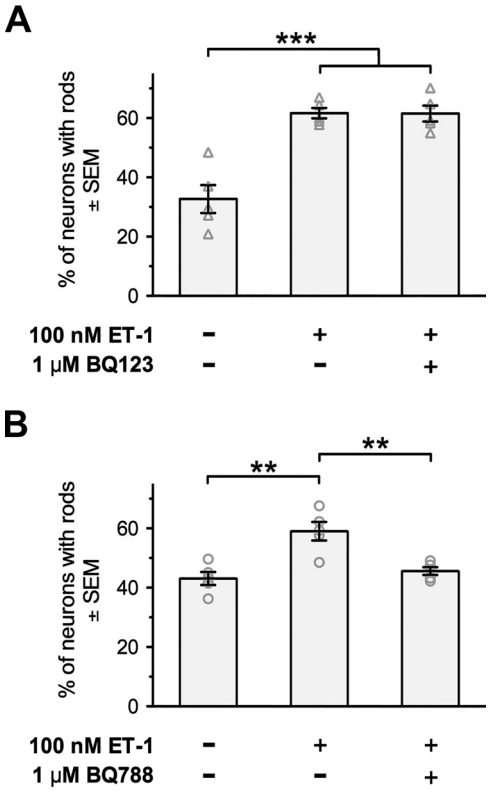

Figure 2. Endothelin type B receptor mediated ET-1–induced cofilin rod formation. Primary hippocampal neurons (14 DIV) were treated with 100 nM ET-1 with or without 1-h pretreatment with 1 μM ET_A antagonist (BQ123) or 1 μM ET_B antagonist (BQ788). Vehicle groups were treated with 0.005% (v/v) acetic acid (*A*) or 0.005% (v/v) acetic acid + 0.1% (v/v) DMSO (*B*). After 24-h treatment, neurons were fixed and stained for cofilin rod quantification. At least 200 neurons were observed for each treatment group per trial. With a total of five trials, at least 1000 neurons were observed for each treatment group. *A* and *B*, quantification of cofilin rod formation shows that pretreatment with BQ788, but not BQ123, abolished ET-1–induced cofilin rod formation. **, $p < 0.01$; ***, $p < 0.001$, one-way ANOVA with Tukey HSD post hoc test. Data were obtained from five independent experiments ($n = 5$). *Error bars* represent S.E.

induced cofilin rod formation via NOX-driven superoxide production. As the first step to test this hypothesis, we examined whether IRL1620 induced superoxide production via NOX by dihydroethidium (DHE) assay. Treatment with 100 nM IRL1620 significantly increased the level of red ethidium signal in neurons, which was abolished by pretreatment with 5 μM NOX inhibitor (VAS2870) (Fig. 6, *C* and *D*), supporting that ET_B activation mediates superoxide formation via NOX. Indeed, pretreatment with 5 μM VAS2870 also abolished IRL1620-induced cofilin rod formation in neurons (Fig. 6*E*). In short, these findings show that ET_B activation induces cofilin rod formation via NOX-mediated superoxide production.

Endothelin type B receptor mediates cofilin rod formation via cofilin activation

A previous study reported that neurons overexpressing WT cofilin or constitutively active cofilin mutant (S3A) formed cofilin rods (16). However, neurons expressing the inactive phosphomimetic cofilin mutant (S3D) did not form cofilin rods, suggesting that overactivation of cofilin also could lead to cofilin rod formation. Activity of cofilin is negatively regulated by phosphorylation at Ser-3 residue. Upon dephosphorylation at Ser-3 residue, cofilin has higher affinity for actin filament. According to a biophysical model (24), when there was high ratio of active cofilin to actin, cofilin would bind to the actin filament in a saturated and symmetrical manner. This would result in stabilization of that actin filament. Subsequent severing at the bare actin filament near the cofilin-overdecorated site led to the formation of a cofilin–actin rod. Therefore, to investigate whether ET_B activation also mediates formation of cofilin–actin rods via cofilin activation, we first examined the expression of actin in IRL1620-induced cofilin rods and the effect of IRL1620 on cofilin activation. Interestingly, we found that actin was expressed in the IRL1620-induced cofilin rods (Fig. 7*A*). Besides, after 24-h treatment with 100 nM IRL1620, the Ser-3 phosphorylation level of cofilin was significantly down-regulated (Fig. 7, *B* and *C*). These results indicate that ET_B activation induces cofilin–actin rod formation and cofilin activation.

In neurons, the level of cofilin activation is tightly regulated. The phosphatase Slingshot homolog 1 (SSH-1L), which is mainly activated by calcineurin (25), is the major phosphatase mediating cofilin activation (26). LIMK1 is the major kinase mediating cofilin inactivation (27). A previous study showed that overexpression of LIMK1 suppressed Aβ-induced cofilin rod formation, whereas overexpression of SSH-1L exacerbated Aβ-induced cofilin rod formation in primary neurons (18). Therefore, we further examined the role of cofilin activation in ET_B activation–induced cofilin rod formation by using a calcineurin inhibitor (FK506) or LIMK1 inhibitor (LIMKi-3). Consistent with the previous study (16), treatment with 100 nM FK506, which presumably suppressed cofilin activation, did not induce significant cofilin rod formation (Fig. 7*D*). However, treatment with 1 μM LIMKi-3, which presumably enhanced cofilin activation, induced significant cofilin rod formation (Fig. 7*E*). Pretreatment with 100 nM FK506, but not 1 μM LIMKi-3, partially abolished IRL1620-induced cofilin rod formation (Fig. 7, *D* and *E*). Hence, these findings showed that IRL1620-induced cofilin rod formation was suppressed by FK506-meditaed cofilin inactivation but not by LIMKi-3–mediated cofilin activation, supporting that ET_B activation also mediates cofilin rod formation via cofilin activation.

Discussion

Although the increased ET-1 level in the brain has long been related to AD neuropathologies, the mechanisms behind it remain elusive. A pathologically high concentration of ET-1 was used in this study to mimic the high level of ET-1 in the AD brain. Here, we showed that a high concentration, *i.e.* 1, 10, or 100 nM, of ET-1, which did not induce significant neuronal cell death (Figs. S1 and S2), led to significant cofilin rod formation in the dendrites of 14-DIV hippocampal neurons. Consistently, cofilin rod formation has been considered as an early neuropathology of AD (17), which leads to blockage of intracellular trafficking and synaptic loss instead of neuronal death (16). This suggested that a high level of ET-1 in the brain might induce neuronal dysfunction in the early stage of AD. The 14-DIV hippocampal neurons expressed both ET_A and ET_B (Fig. S3). Using a pharmacological approach, we further demonstrated that ET-1 induced cofilin rod formation, loss of distal

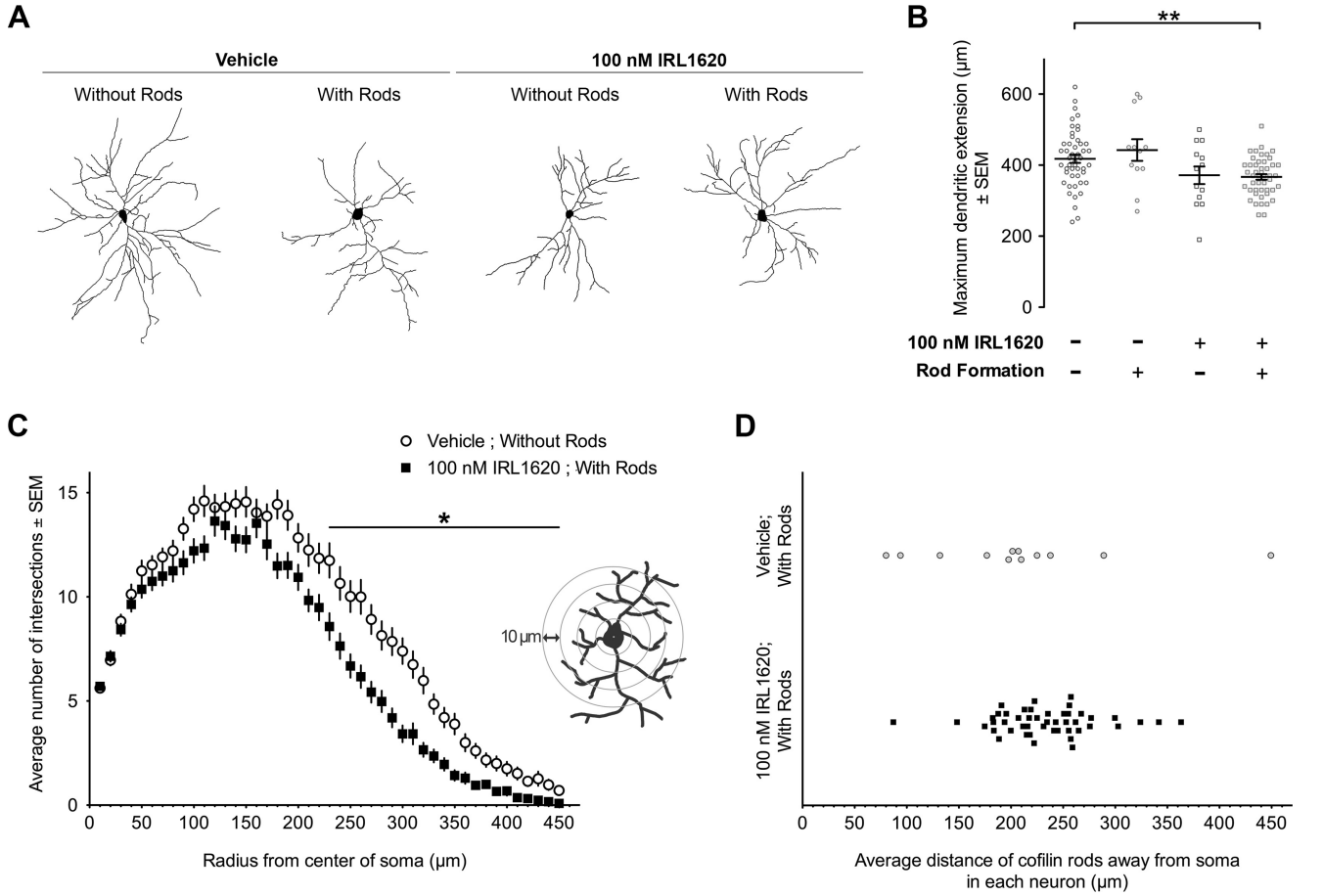

Figure 3. Endothelin type B receptor agonist–induced cofilin rod formation was accompanied by the loss of distal dendrites. Primary hippocampal neurons were treated with vehicle or 100 nM selective ET_B agonist (IRL1620) at 14 DIV. After 24-h treatment, neurons were fixed for double immunofluorescence staining of MAP2 and cofilin. For dendritic morphological analysis, a total of 60 individual neurons, which were pooled from three independent trials, were analyzed for each treatment group. Based on the presence of cofilin rods, the vehicle-treated and IRL1620-treated neurons were subdivided into two groups: without rods and with rods. The MAP2-positive dendritic network was subjected to neurite tracing for further analysis of dendritic morphology. *A*, representative neurite tracing results of neurons in each group. *B*, quantification of maximum extension radius of the dendritic network. **, $p < 0.01$, Welch's ANOVA with Dunnett's T3 post hoc test; $n = 12$ and 48 for vehicle-treated neurons with and without rods, respectively; $n = 47$ and 13 for IRL1620-treated neurons with and without rods, respectively. *C*, the Sholl plot of vehicle-treated neurons without rods ($n = 48$) and IRL1620-treated neurons with rods ($n = 47$). Compared with the vehicle-treated neurons without rods, the IRL1620-treated neurons with rods showed significant reduction in the number of intersections at 230–450 μm away from the soma. *, $p < 0.05$, Welch's ANOVA with Dunnett's T3 post hoc test. *D*, the distribution pattern of cofilin rods in the vehicle-treated ($n = 12$) and IRL1620-treated ($n = 47$) neurons. Most of the cofilin rods (85%) in the IRL1620-treated neurons were localized at 175–275 μm away from the soma. *Error bars* represent S.E.

dendrites, and reduction in dendritic length via ET_B. Activation of ET_B could induce cofilin rod formation via two different pathways, the oxidative stress pathway and cofilin activation. Treatment with a selective ET_B agonist induced NOX-driven superoxide formation and cofilin activation. Inhibition of either NOX or cofilin activation suppressed ET_B agonist–induced cofilin rod formation. Our study therefore is the first to report that ET_B mediated cofilin rod formation and dendritic loss by oxidative stress and cofilin overactivation in hippocampal neurons (Fig. 8), providing new insight into the possible roles of ET-1 in neurodegeneration.

Previous studies suggested that cofilin rod formation could be one of the mechanisms mediating neurodegeneration during AD progression (17–20). Interestingly, we found that the time course and mechanism of ET-1–induced cofilin rod formation were similar to those reported for Aβ-induced cofilin rod formation. Similar to the effect of Aβ (18), neurons treated with ET-1 started to form cofilin rods after 1 h of treatment and maintained persistently high level of cofilin rod formation after 24 h of treatment. In addition, two separate studies reported that Aβ could induce cofilin rod formation in neurons via either NOX-driven oxidative stress or cofilin activation (18, 21). These findings further establish that ET-1 exerts a neurotoxic effect via cofilin rod formation. It would be interesting to further investigate the potential synergistic effect of ET-1 and Aβ on mediating cofilin rod formation and subsequent neuronal dysfunction.

This study has demonstrated that ET_B activation–induced cofilin rods were located distally, which was in line with their roles in mediating the loss of distal dendrites. Consistent with this finding, a previous study also reported that distal dendrites have a lower ATP/ADP ratio and a higher degree of oxidation in mitochondria and cytosol compared with the proximal dendrites or the soma (28), making the distal dendrites more prone to cofilin rod formation. The mechanism behind cofilin rod–induced loss of dendrites has not yet been demonstrated. However, a previous study showed that cofilin rods induced synaptic loss and blocked intracellular trafficking of mitochondria and

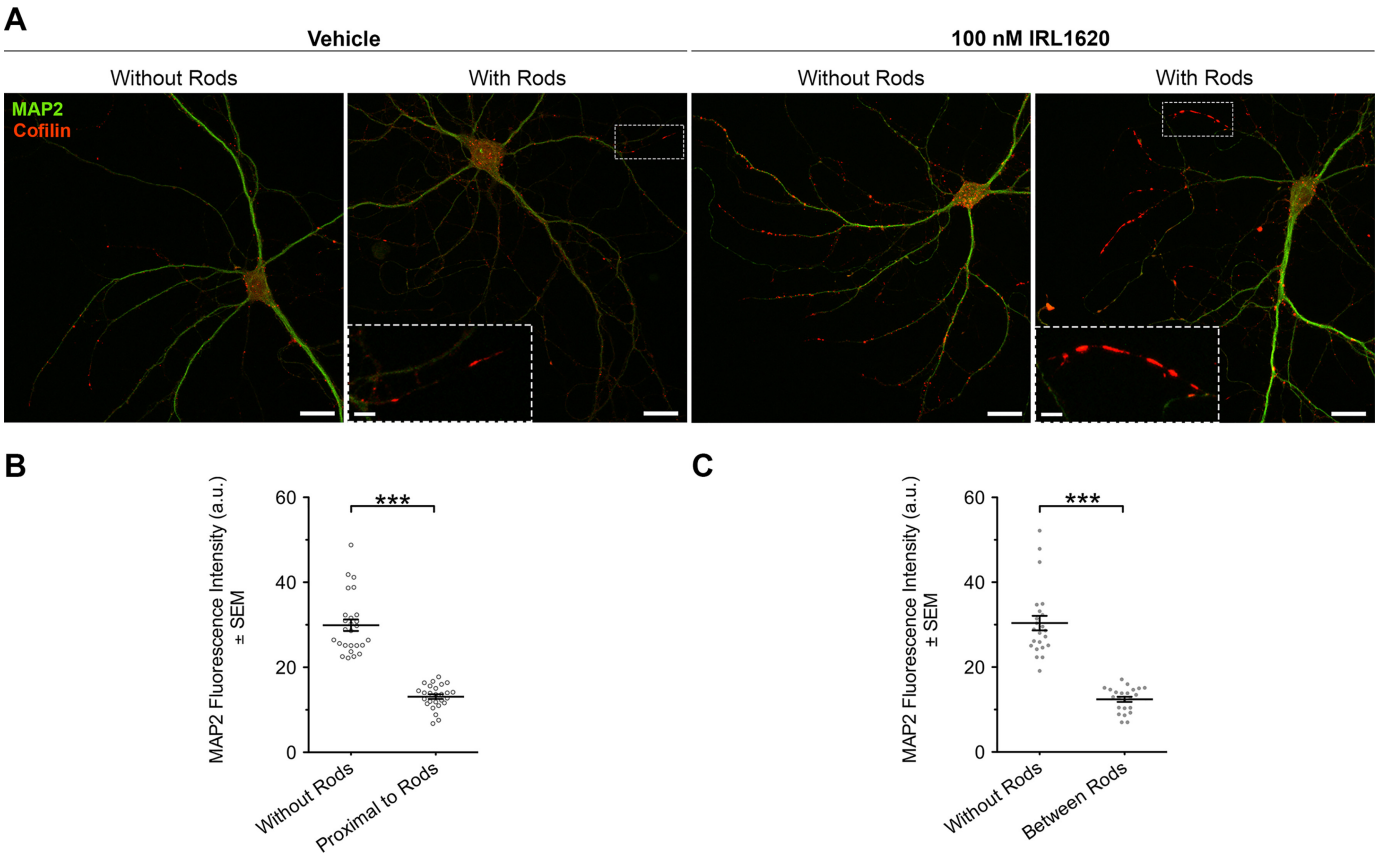

Figure 4. Reduction in MAP2 signals was observed around the ET_B agonist–induced cofilin rods. Primary hippocampal neurons were treated with vehicle or 100 nM selective ET_B agonist (IRL1620) at 14 DIV. After 24-h treatment, neurons were fixed for double immunofluorescence staining of MAP2 and cofilin. Neurons with and without cofilin rod formation were both observed in the vehicle and IRL1620 treatment groups. *A*, representative confocal images show the double immunofluorescence staining of MAP2 (*green*) and cofilin (*red*) in neurons treated with vehicle or IRL1620. Enlarged views show the reduced MAP2 signal around cofilin rods in the distal dendrites. *B* and *C*, quantification of MAP2 intensity at 2.5 μm before the most proximal cofilin rods (*B*) and between the cofilin rods (*C*) in the IRL1620-treated neurons. The average MAP2 intensities at the same distance away from the soma in the rod-negative dendrites of the same neurons were measured as the baseline level. ***, $p < 0.001$, two-tailed independent *t* test. A total of 87 dendrites from 28 IRL1620-treated neurons were analyzed. Analyzed data were obtained from 28 (*B*) and 25 (*C*) individual neurons pooled from three independent experiments (*B*, $n = 28$; *C*, $n = 25$). *Scale bars*, 20 μm (5 μm in *enlarged views*). *a.u.*, arbitrary units. *Error bars* represent S.E.

vesicles in dendrites (16). The same study also well-demonstrated that dendrites with cofilin rods had significantly lower synaptic activity compared with dendrites without cofilin rods in the same neuron. Loss of synaptic input could lead to loss of dendrites *in vivo* (29), suggesting that synaptic loss could be one of the mechanisms of how ET_B activation–induced cofilin rods lead to loss of distal dendrites. In contrast, cofilin rod–mediated blockage of intracellular trafficking in dendrites might inhibit the fusion of mitochondria, which further promotes the local accumulation of reactive oxygen species and possibly leads to a positive feedback on oxidative stress–driven cofilin rod formation in the distal dendrites. Supporting this idea, it was reported that aberrantly round-shaped mitochondria were observed in dendrites with cofilin rods but not in dendrites without cofilin rods (16). Moreover, blockage of intracellular trafficking might also inhibit the turnover of cytoskeletal elements, such as those in the microtubule system. A previous study showed the loss of tubulin around the cofilin rod–occupied area in neurites (22). Similarly, we also demonstrated the loss of MAP2, which binds and stabilizes microtubules in neurons, around the cofilin rods in dendrites. These results support the roles of cofilin rods in disrupting the microtubule system and its subsequent impact causing the degeneration of distal dendrites.

Given that ET_B mediates cofilin rod formation via oxidation and activation of cofilin (Figs. 6 and 7), it is possible that ET_B also mediates other cofilin dysregulation–induced neuronal dysfunctions via cofilin rod–independent pathways. The results of this study suggest that ET_B activation induces length reduction in 2°–4° dendrites via a cofilin rod–independent pathway, although the mechanisms remained elusive. Because ET_B was shown to mediate cofilin activation, it is possible that ET_B activation could lead to dysregulation of the local actin dynamics, resulting in the loss of synapses and dendrites. Indeed, cofilin-regulated actin dynamics is essential for modulating the structure of actin-rich postsynaptic dendritic spines (30). Overactivation of cofilin in neurons was reported to destabilize mature synapses as shown by the aberrantly high proportion of filopodial protrusions and small dendritic head size in the neurons expressing active cofilin mutant (S3A) (31). In contrast, oxidation on Cys-39 and Cys-147 residues of cofilin induced formation of intermolecular disulfide bonds, which were essential for formation of cofilin rods (15). However, a different cysteine oxidation pattern on cofilin could lead to formation of intramolecular disulfide bonds and subsequent mito-

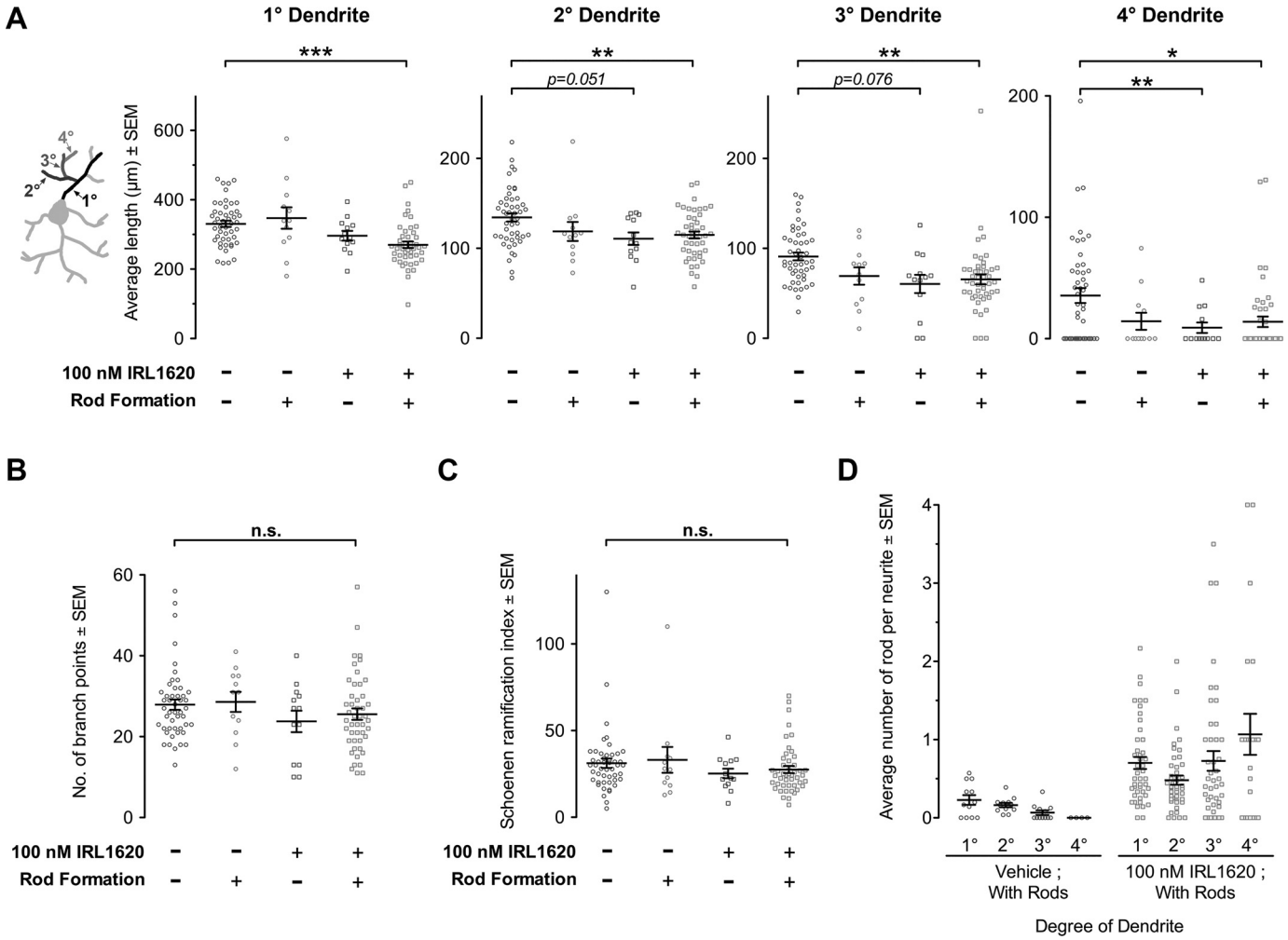

Figure 5. The ET_B agonist–treated neurons with cofilin rods showed significant reduction in dendritic length but no significant change in branching or ramification. Primary hippocampal neurons were treated with vehicle or 100 nM selective ET_B agonist (IRL1620) at 14 DIV. After 24-h treatment, neurons were fixed for double immunofluorescence staining of MAP2 and cofilin. For dendritic morphological analysis, a total of 60 individual neurons, which were pooled from three independent trials, were analyzed for each treatment group. Based on the presence of cofilin rods, the vehicle-treated and IRL1620-treated neurons were subdivided into two groups: without rods and with rods. The MAP2-positive dendritic network was subjected to neurite tracing for further analysis of dendritic morphology. *A–C*, quantification of average length of 1°–4° dendrites (*A*), number of branch points (*B*), and Schoenen ramification index (radius with the maximum number of intersection/total number of 1° dendrites; *C*). *, $p < 0.05$; **, $p < 0.01$; ***, $p < 0.001$, Welch's ANOVA with Dunnett's T3 post hoc test; $n = 12$ and 48 for vehicle-treated neurons with and without rods, respectively; $n = 47$ and 13 for IRL1620-treated neurons with and without rods, respectively. *D*, the distribution pattern of cofilin rods in 1°–4° dendrites of vehicle-treated ($n = 12$) and IRL1620-treated neurons ($n = 47$). Cofilin rods in IRL1620-treated neurons were found in 1°–4° dendrites. *Error bars* represent S.E.

chondrial translocation of cofilin, which could lead to mitochondrial dysfunction and mitochondrial oxidative stress (15, 32). Therefore, further studies are needed to elucidate whether ET_B activation can disrupt actin dynamics and induce dysfunction of synapses and mitochondria.

In the past decade, Gulati and co-workers (33, 36–37) proposed ET receptor as a potential therapeutic target for treating AD. Using the intracerebroventricular $A\beta_{1-40}$-perfused rats as an AD model, they reported that intracerebroventricular perfusion of the ET_A antagonist BQ123 reduced oxidative stress in the brain and rescued performance decline in memory-based tasks (33), possibly by protecting the integrity of the blood–brain barrier and preventing vascular oxidative stress (34, 35). Notably, using the same AD rat model, they also reported that the ET_B agonist IRL1620 rescued $A\beta_{1-40}$-induced performance decline in the Morris water maze test regardless of whether IRL1620 was administrated by intracerebroventricular perfusion or intravenous injection (36, 37). Presumably, IRL1620 could not pass through the blood–brain barrier. Without getting into the brain, the intravenously injected IRL1620 was proposed to exert its neuroprotective effect by increasing the level of vascular endothelial growth factor and nerve growth factor in the brain (36). Getting into the brain, the intracerebroventricularly perfused IRL1620 was proposed to exert its neuroprotective effect by suppressing the $A\beta_{1-40}$-induced up-regulation of oxidative stress markers in the brain (37). Besides neural cells, ET_B is also expressed by astrocytes, endothelial cells, and activated microglia in the brain (4, 8, 38). Interestingly, $A\beta$ has been associated with oxidative stress in these four cell types in the brain (39–41), suggesting that ET_B activation might alleviate $A\beta$-induced oxidative stress in different cell types in the brain and rescue $A\beta$-induced cognitive decline. To further consolidate this idea, in a future study, viability and morphology of primary neurons shall be examined after being cocultured with

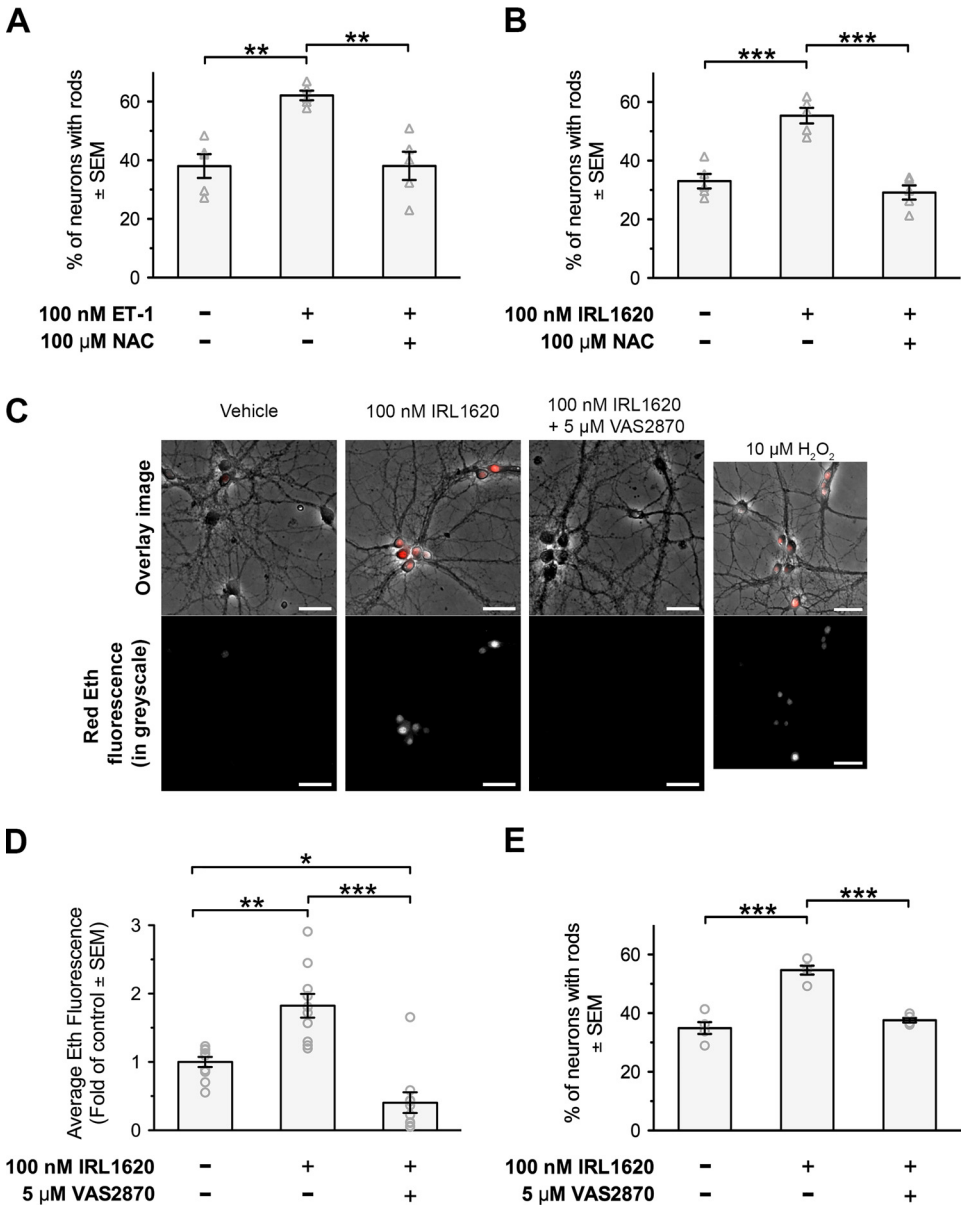

Figure 6. Endothelin type B receptor mediated cofilin rod formation in hippocampal neurons via NADPH oxidase–mediated superoxide production. *A*, *B*, and *E*, primary hippocampal neurons (14 DIV) were treated for 24 h. After treatment, neurons were fixed and stained for cofilin rod quantification. At least 200 neurons were observed for each treatment group per trial. With a total of five trials, at least 1000 neurons were observed for each treatment group. *A* and *B*, quantification of cofilin rod formation in neurons treated with 100 nM ET-1 or 100 nM selective ET_B agonist (IRL1620) with or without cotreatment with 100 μM antioxidant NAC. The vehicle group for ET-1 treatment was treated with 0.005% (v/v) acetic acid (*A*). **, $p < 0.01$; ***, $p < 0.001$, one-way ANOVA with Tukey HSD post hoc test. Data were obtained from five independent experiments ($n = 5$). *C* and *D*, hippocampal neurons (14 DIV) were preincubated with 5 μM DHE, which emits red Eth fluorescence upon superoxide-driven conversion. DHE-preloaded neurons were treated with 100 nM IRL1620 with or without 30-min pretreatment with 5 μM NADPH oxidase inhibitor (VAS2870). The vehicle group was treated with 0.1% (v/v) DMSO. After 4-h treatment, neurons were imaged under an epifluorescence microscope, and the intensity of Eth fluorescence was quantified. *C*, representative overlay images of Eth fluorescence (*red*) and corresponding phase-contrast images of neurons. A sublethal concentration (10 μM) of H_2O_2, which induces cofilin rod formation after 24-h treatment (data not shown), served as a positive control. *D*, quantification of Eth fluorescence. *, $p < 0.05$; **, $p < 0.01$; ***, $p < 0.001$, one-way ANOVA with Tukey HSD post hoc test. Data were obtained from 10 independent experiments ($n = 10$). *E*, quantification of cofilin rod formation in neurons treated with 100 nM IRL1620 with or without 30-min pretreatment with 5 μM VAS2870. The vehicle group was treated with 0.1% (v/v) DMSO. ***, $p < 0.001$, one-way ANOVA with Tukey HSD post hoc test. Data were obtained from five independent experiments ($n = 5$). *Scale bars*, 100 μm. *Error bars* represent S.E.

astrocytes, microglia, or endothelial cells treated with Aβ, ET_B agonist, or both. Given that ET_B agonist has been proposed as a potential therapeutic target for delaying AD progression, the current study provides new insight into the potential adverse effects of ET_B agonist on mature neurons. Further investigations are warranted for studying other potential side effects of ET receptor agonist or antagonist in the brain.

Experimental procedures

Primary hippocampal neuronal culture and pharmacological treatment

All cell culture reagents were purchased from Invitrogen unless otherwise specified. Primary hippocampal neurons were prepared from embryonic day 16.5 embryos of C57BL/6N mice

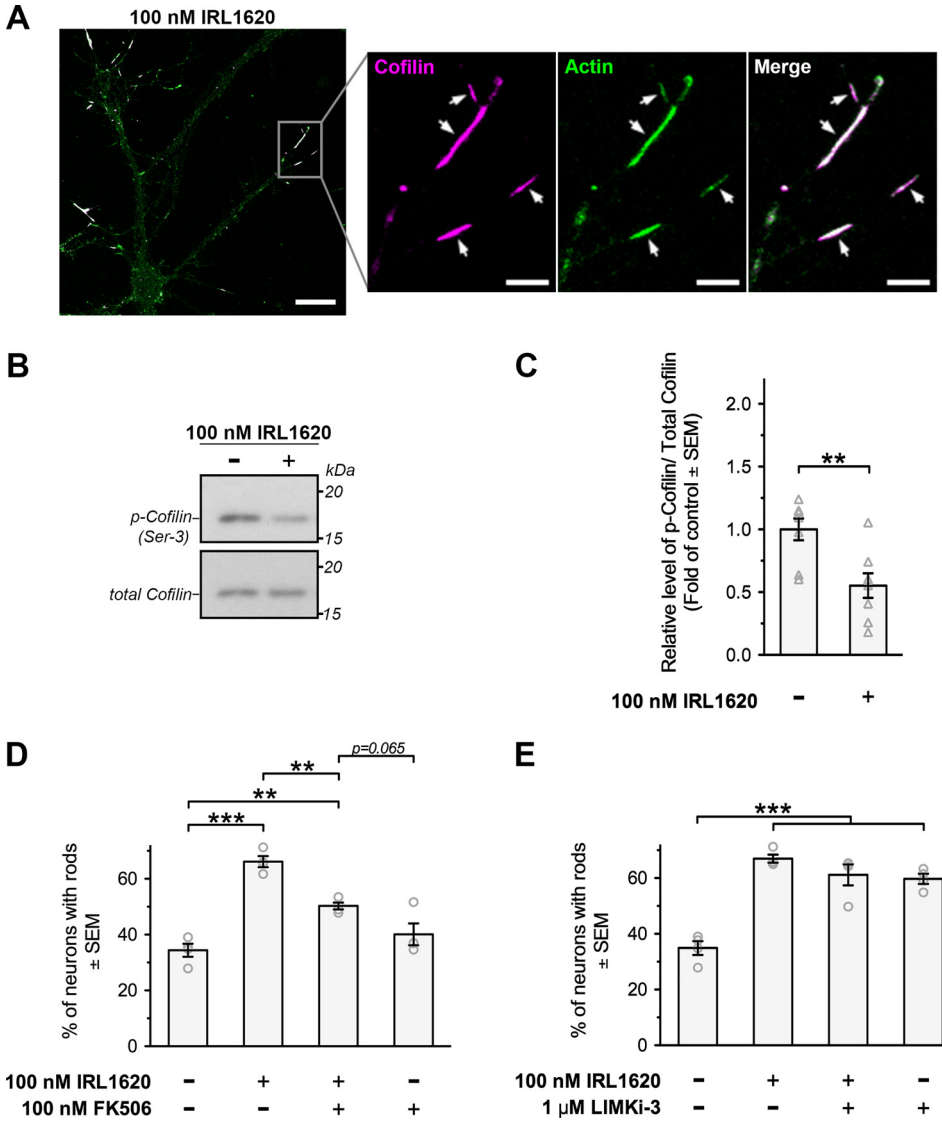

Figure 7. Endothelin type B receptor mediated cofilin–actin rod formation in hippocampal neurons by mediating cofilin dephosphorylation. Primary hippocampal neurons (14 DIV) were treated with 100 nM selective ET_B agonist (IRL1620) with or without 1-h pretreatment with 100 nM calcineurin inhibitor (FK506) or 1 μM LIMK1 inhibitor (LIMKi-3). Vehicle groups for FK506 or LIMKi-3 treatment were treated with 0.01% (v/v) DMSO (*D–G*). After 24-h treatment, neurons were fixed for immunofluorescence staining, or proteins harvested from whole-cell lysate were subjected to Western blot analysis. *A*, representative confocal images showed the double immunofluorescence staining of cofilin (*magenta*) and actin (*green*) in the IRL1620-treated neurons. Actin was expressed in the IRL1620-induced cofilin rods (*arrows*). Observation was based on 30 neurons pooled from four independent experiments. *B* and *C*, representative blots and quantification of Ser-3 phosphorylation level of cofilin in neurons treated with IRL1620. **, $p < 0.01$, two-tailed independent *t* test. Data were obtained from eight independent experiments ($n = 8$). *D* and *E*, quantification of cofilin rod formation in neurons treated with IRL1620 with or without pretreatment with FK506 or LIMKi-3. At least 200 neurons were observed for each treatment group per trial. With a total of four trials, at least 800 neurons were observed for each treatment group. **, $p < 0.01$; ***, $p < 0.001$, one-way ANOVA with Tukey HSD post hoc test. Data were obtained from four independent experiments ($n = 4$). *Scale bars*, 20 μm (5 μm in *enlarged views*). *Error bars* represent S.E.

according to a reported protocol with optimization (42). The experimental protocol was approved by the Committee on the Use of Live Animals in Teaching and Research (reference number 3362-14) of The University of Hong Kong. In brief, hippocampal tissues were dissociated by 8-min enzymatic digestion with 0.0625% (v/v) trypsin-EDTA solution at 37 °C followed by trituration. Dissociated hippocampal neurons were seeded on 14-mm round coverslips, 4-well plates, or 6-well plates coated with 50 μg/ml poly-D-lysine (Sigma) at low density (0.15×10^5 cells/coverslip for immunofluorescence staining; 0.3×10^5 cells/well in 4-well plates for DHE assay) or at high density (3.5×10^5 cells/well in 6-well plates for Western blot analysis) in Neurobasal medium supplemented with 2% (v/v) B27, 2 mM GlutaMAX, 50 units/ml penicillin–streptomycin, and 25 μM glutamate (Sigma). After 24 h of seeding, one-third of the glutamate-containing medium was replaced by a double volume of glutamate-free supplemented Neurobasal medium. Neurons were treated with 1 μM 5-fluoro-5′-deoxyuridine (Sigma) at 5 DIV for facilitating the removal of glial cells. Medium was changed at 5, 9, and 12 DIV. Neurons were pharmacologically treated at 14 DIV without replacing with fresh supplemented Neurobasal medium.

The chemicals for pharmacological treatment of neurons were purchased from Sigma except FK506 and LIMKi-3, which were from Tocris Bioscience. Endothelin-1 was prepared as a 200× stock in 1% acetic acid. The stock solutions of BQ123

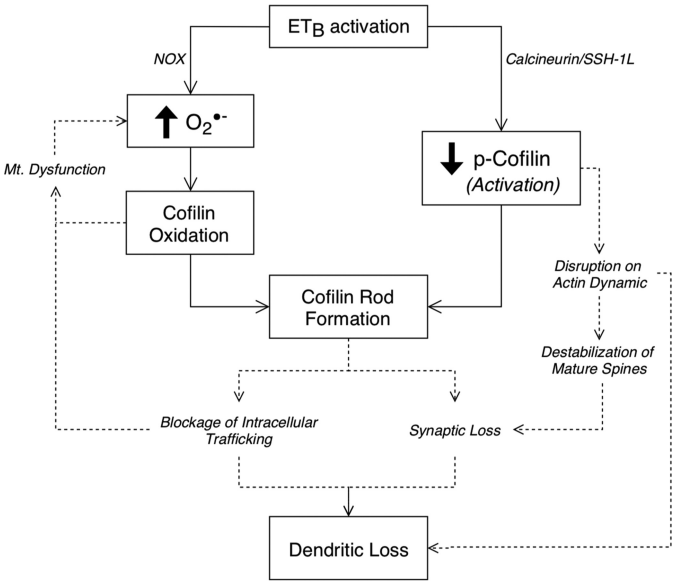

Figure 8. Schematic diagram summarizing the potential mechanisms behind ET_B-mediated cofilin rod formation and dendritic loss in primary hippocampal neurons. Our study has demonstrated that ET_B activation induced cofilin rod formation via NOX-mediated oxidative stress pathway and calcineurin/SSH-1L–mediated cofilin activation. According to previous studies, cofilin rod formation leads to loss of distal dendrites, possibly by blocking the intracellular trafficking and inducing loss of synapse and reduction of synaptic activity in neurites. In the meantime, the cofilin rod–mediated blockage of intracellular trafficking might lead to mitochondrial (*Mt.*) dysfunction, for example, by prohibiting the fusion of mitochondria, which further enhances the accumulation of reactive oxygen species in the distal dendrites. In contrast, ET_B activation might also induce loss of synapse and dendrite via a cofilin rod–independent pathway. For instance, here, we have demonstrated that ET_B activation leads to cofilin activation. The aberrant cofilin activation might disrupt local actin dynamics, leading to destabilization of mature dendritic spines and shortening of dendrites. *Solid lines* indicate the results reported in this study. *Dotted lines* indicate the possible pathways in accordance with previous studies discussed under "Discussion."

(1000×), IRL1620 (200×), NAC (100×), and hydrogen peroxide (H_2O_2; 100×) were prepared in Neurobasal medium. The stock solutions of BQ788 (1000×), VAS2870 (1000×), FK506 (10,000×), and LIMKi-3 (10,000×) were prepared in sterile-filtered DMSO (Sigma).

Quantification of superoxide production

After rinsing once with prewarmed incubation buffer (Hank's balance salt solution with 0.8 mM magnesium sulfate, 1.2 mM calcium chloride, 25 mM D-glucose, and 3% (w/v) sucrose), neurons were pretreated with vehicle or VAS2870 for 30 min and incubated with 5 μM DHE (Invitrogen) for 10–15 min before being treated with IRL1620. After 4-h treatment, the ethidium (Eth) signals (red fluorescence with peak emission wavelength at 580 nm) were captured under a 20× (NA, 0.40) objective of a Nikon TE300 epifluorescence microscope by using a tetramethylrhodamine (TRITC) filter set (excitation filter, 540/25; emission filter, 605/55) and 2-s exposure time. Corresponding phase-contrast images were captured for outlining the soma during quantification. The intensity of Eth fluorescence was quantified using Fiji software and normalized by the area of the soma. For each treatment group, five randomly chosen microscopic fields were captured from one of the 3–4 wells per trial.

Immunofluorescence staining

After pharmacological treatment, cofilin rods in neurons were visualized by immunofluorescence staining according to previous studies (16, 18). In brief, neurons were fixed by 4% (w/v) paraformaldehyde for 45 min at room temperature. After washing with PBS, fixed neurons were permeabilized by ice-cold absolute methanol for 3 min at −20 °C. After rinsing with PBS, neurons were incubated with blocking buffer (10% BSA (w/v) in PBS) for 1 h at room temperature and then incubated with primary antibody (cofilin, rabbit monoclonal, catalog number 5175, 1:1000; MAP2, rabbit polyclonal, catalog number 4542, 1:400; tau, mouse monoclonal, catalog number 4019, 1:500, Cell Signaling Technology; actin, mouse monoclonal, catalog number YM3028, 1:1000, ImmunoWay) in universal antibody diluent (Abcam) overnight at 4 °C. Neurons were washed three times with washing buffer (0.01% Triton X-100 (v/v) in PBS) and then incubated with Alexa Fluor–conjugated secondary antibody (1:1000 in PBS) for 1 h at room temperature. For the double immunofluorescence staining of MAP2 and cofilin, of which primary antibodies were raised from rabbit, excess FITC-conjugated monovalent Fab anti-rabbit secondary antibody (1:250 in 5% (w/v) BSA; Abcam) was used to tag the first MAP2 primary antibody. Upon thorough washing with washing buffer, neurons were subsequently incubated with cofilin primary antibody (1:1000 in universal antibody diluent) overnight at 4 °C and with Alexa Fluor 568– or 647–conjugated anti-rabbit secondary antibody (1:1000 in PBS) for 1 h at room temperature on the next day. Following nuclear counterstaining (0.25 μg/ml 4′,6-diamidino-2-phenylindole (DAPI) in PBS; Cell Signaling Technology) and washing three times in washing buffer, stained neurons were mounted with ProLong Diamond antifade mounting solution (Invitrogen) and healed in the dark for at least 4 days before visualizing under an epifluorescence or confocal microscope. All confocal images were captured under a 40× (NA, 1.40) oil-immersion objective of a Carl Zeiss LSM710 confocal microscope installed with Zen Black digital imaging software.

Quantification of cofilin rod formation

Immunofluorescence staining of cofilin in neurons was visualized under a 40× (NA, 0.75) objective of an Olympus CKX41 epifluorescence microscope. According to the previous study (16), a cofilin rod was defined as a cofilin-positive rod-shaped structure that was at least 3 μm in length and was located in a neurite. The cofilin rods observed in this study typically had a width of 0.5–1 μm. Neurons were identified as rod-positive if they presented at least one cofilin rod in a neurite. The average number of rods per neuron, which was also named as the rod index in a previous study (21), was calculated as the ratio of the number of rods/number of somata in each microscopic field. Cofilin rod analysis was done in a blinded manner. Randomly coded coverslips were not identified until all coverslips in one trial had been analyzed. At least 200 neurons from 60–70 randomly chosen microscopic fields were counted for each treatment group per trial. With a total of four to five independent trials, at least 800–1000 neurons were analyzed for each treatment group.

Quantification of dendritic morphology and MAP2 intensity in dendrites

The double immunofluorescence staining of MAP2 and cofilin in neurons was captured under a 20× (NA, 0.4) objective of an Olympus CKX41 epifluorescence microscope. Captured images were quantified using Fiji software. For neurons having an extensive dendritic network, multiple images of a single neuron were stitched by the 2D stitching plug-in. For quantification of dendritic morphology, the images of MAP2 staining were segmented by thresholding and subjected to neurite tracing by using the "simple neurite tracer" plug-in. The center of the soma was set as the starting point of all 1° dendrites. Sholl analysis was done using a 10-μm-radius difference between consecutive circles. Neurite arborization was shown by Schoenen ramification index (radius with maximum number of intersection/total number of 1° dendrites) and the total number of branch points. Dendrites were subdivided into 1°–4° dendrites in which 1° dendrites were defined as the direct extension from the soma, 2° dendrites were defined as the direct extension from the 1° dendrites, etc. For the quantification of MAP2 intensity in dendrites of the IRL1620-treated neurons with cofilin rods, the MAP2 intensity at 2.5 μm before the most proximal cofilin rods was measured. If there were more than one cofilin rod in one dendrite, the MAP2 intensity at 2.5 μm before the most distal cofilin rod was also measured and referred to as the MAP2 intensity in the between-rods region. The average MAP2 intensities at the same distance away from the soma in the rod-negative dendrites of the same neurons were measured as the baseline level.

Western blot analysis

Neurons were lysed in radioimmunoprecipitation assay (RIPA) buffer containing 1 mM phenylmethylsulfonyl fluoride, 10% (v/v) protease inhibitor mixture (Sigma), and 1% (v/v) phosphatase inhibitor mixture 2 (Sigma). The lysate was incubated for 90 min at 4 °C with agitation and cleared of cell debris by centrifugation at 14,000 × *g* for 15 min at 4 °C. The protein extract was boiled in 4× sample buffer (240 mM Tris-Cl, pH 6.80, 40% (v/v) glycerol, 8% (w/v) SDS, 0.04% (w/v) bromphenol blue, and 10% (v/v) β-mercaptoethanol) for 5 min, separated by 12% SDS-PAGE, and transferred onto polyvinylidene difluoride membrane. Following blocking in 5% (w/v) nonfat milk in TBST for 1 h at room temperature, the membrane was incubated with primary antibodies (p-cofilin (Ser-3), rabbit monoclonal, catalog number 3313, 1:1000; cofilin, rabbit monoclonal, catalog number 5175, 1:10,000; Cell Signaling Technology; diluted in 5% (w/v) BSA in TBST) overnight at 4 °C. After washing three times with TBST, the membrane was incubated with horseradish peroxidase (HRP)-conjugated anti-rabbit secondary antibodies (diluted in 5% (w/v) nonfat milk in TBST) for 1 h at room temperature. The HRP signal was detected by Immobilon Western Chemiluminescent HRP Substrate (EMD Millipore) and quantified by densitometry using Fiji software. After probing for p-cofilin, the membrane was stripped by incubating with a mild stripping buffer (200 mM glycine, 0.1% (w/v) SDS, and 1% (v/v) Tween 20, pH 2.20) for 10 min twice at room temperature before probing for the total cofilin.

Statistical analysis

Statistical analyses were conducted in SPSS Statistics version 22. Numerical data were represented as mean ± S.E. Group mean differences were analyzed using two-tailed independent *t* test, one-way ANOVA with Tukey HSD post hoc test, or Welch's ANOVA with Dunnett's T3 post hoc test where appropriate.

Author contributions—S.-W. T. conceptualization; S.-W. T. data curation; S.-W. T. formal analysis; S.-W. T. investigation; S.-W. T. methodology; S.-W. T. writing-original draft; S.-W. T., R. F., W. K.-W. L., A. C.-K. L., P. K.-K. Y., and S. K. C. writing-review and editing; A. C.-K. L. and S. K. C. supervision; A. C.-K. L. and S. K. C. funding acquisition.

References

1. Minami, M., Kimura, M., Iwamoto, N., and Arai, H. (1995) Endothelin-1-like immunoreactivity in cerebral cortex of Alzheimer-type dementia. *Prog. Neuropsychopharmacol. Biol. Psychiatry* **19,** 509–513 CrossRef Medline
2. Palmer, J. C., Barker, R., Kehoe, P. G., and Love, S. (2012) Endothelin-1 is elevated in Alzheimer's disease and upregulated by amyloid-β. *J. Alzheimers Dis.* **29,** 853–861 CrossRef Medline
3. Zhang, W. W., Badonic, T., Höög, A., Jiang, M. H., Ma, K. C., Nie, X. J., and Olsson, Y. (1994) Astrocytes in Alzheimer's disease express immunoreactivity to the vaso-constrictor endothelin-1. *J. Neurol. Sci.* **122,** 90–96 CrossRef Medline
4. Gadea, A., Schinelli, S., and Gallo, V. (2008) Endothelin-1 regulates astrocyte proliferation and reactive gliosis via a JNK/c-Jun signaling pathway. *J. Neurosci.* **28,** 2394–2408 CrossRef Medline
5. Carter, S. F., Schöll, M., Almkvist, O., Wall, A., Engler, H., Långström, B., and Nordberg, A. (2012) Evidence for astrocytosis in prodromal Alzheimer disease provided by ^{11}C-deuterium-L-deprenyl: a multitracer PET paradigm combining ^{11}C-Pittsburgh compound B and ^{18}F-FDG. *J. Nucl. Med.* **53,** 37–46 CrossRef Medline
6. Heneka, M. T., Sastre, M., Dumitrescu-Ozimek, L., Dewachter, I., Walter, J., Klockgether, T., and Van Leuven, F. (2005) Focal glial activation coincides with increased BACE1 activation and precedes amyloid plaque deposition in APP[V717I] transgenic mice. *J. Neuroinflammation* **2,** 22 CrossRef Medline
7. Olabarria, M., Noristani, H. N., Verkhratsky, A., and Rodríguez, J. J. (2010) Concomitant astroglial atrophy and astrogliosis in a triple transgenic animal model of Alzheimer's disease. *Glia* **58,** 831–838 CrossRef Medline
8. Naidoo, V., Naidoo, S., Mahabeer, R., and Raidoo, D. M. (2004) Cellular distribution of the endothelin system in the human brain. *J. Chem. Neuroanat.* **27,** 87–98 CrossRef Medline
9. Dong, F., Zhang, X., Wold, L. E., Ren, Q., Zhang, Z., and Ren, J. (2005) Endothelin-1 enhances oxidative stress, cell proliferation and reduces apoptosis in human umbilical vein endothelial cells: role of ETB receptor, NADPH oxidase and caveolin-1. *Br. J. Pharmacol.* **145,** 323–333 CrossRef Medline
10. Li, L., Fink, G. D., Watts, S. W., Northcott, C. A., Galligan, J. J., Pagano, P. J., and Chen, A. F. (2003) Endothelin-1 increases vascular superoxide via endothelin$_A$-NADPH oxidase pathway in low-renin hypertension. *Circulation* **107,** 1053–1058 CrossRef Medline
11. Koyama, Y., and Baba, A. (1996) Endothelin-induced cytoskeletal actin re-organization in cultured astrocytes: inhibition by C3 ADP-ribosyltransferase. *Glia* **16,** 342–350 CrossRef Medline
12. Morigi, M., Buelli, S., Zanchi, C., Longaretti, L., Macconi, D., Benigni, A., Moioli, D., Remuzzi, G., and Zoja, C. (2006) Shigatoxin-induced endothelin-1 expression in cultured podocytes autocrinally mediates actin remodeling. *Am. J. Pathol.* **169,** 1965–1975 CrossRef Medline
13. Sato, Y., Hogg, J. C., English, D., and van Eeden, S. F. (2000) Endothelin-1 changes polymorphonuclear leukocytes' deformability and CD11b ex-

pression and promotes their retention in the lung. *Am. J. Respir. Cell Mol. Biol.* **23,** 404–410 CrossRef Medline

14. Semprucci, E., Tocci, P., Cianfrocca, R., Sestito, R., Caprara, V., Veglione, M., Castro, V. D., Spadaro, F., Ferrandina, G., Bagnato, A., and Rosanò, L. (2016) Endothelin A receptor drives invadopodia function and cell motility through the β-arrestin/PDZ-RhoGEF pathway in ovarian carcinoma. *Oncogene* **35,** 3432–3442 CrossRef Medline
15. Bernstein, B. W., Shaw, A. E., Minamide, L. S., Pak, C. W., and Bamburg, J. R. (2012) Incorporation of cofilin into rods depends on disulfide intermolecular bonds: implications for actin regulation and neurodegenerative disease. *J. Neurosci.* **32,** 6670–6681 CrossRef Medline
16. Cichon, J., Sun, C., Chen, B., Jiang, M., Chen, X. A., Sun, Y., Wang, Y., and Chen, G. (2012) Cofilin aggregation blocks intracellular trafficking and induces synaptic loss in hippocampal neurons. *J. Biol. Chem.* **287,** 3919–3929 CrossRef Medline
17. Rahman, T., Davies, D. S., Tannenberg, R. K., Fok, S., Shepherd, C., Dodd, P. R., Cullen, K. M., and Goldsbury, C. (2014) Cofilin rods and aggregates concur with tau pathology and the development of Alzheimer's disease. *J. Alzheimers Dis.* **42,** 1443–1460 CrossRef Medline
18. Davis, R. C., Marsden, I. T., Maloney, M. T., Minamide, L. S., Podlisny, M., Selkoe, D. J., and Bamburg, J. R. (2011) Amyloid β dimers/trimers potently induce cofilin-actin rods that are inhibited by maintaining cofilin-phosphorylation. *Mol. Neurodegener.* **6,** 10 CrossRef Medline
19. Minton, A. Z., Phatak, N. R., Stankowska, D. L., He, S., Ma, H. Y., Mueller, B. H., Jiang, M., Luedtke, R., Yang, S., Brownlee, C., and Krishnamoorthy, R. R. (2012) Endothelin B receptors contribute to retinal ganglion cell loss in a rat model of glaucoma. *PLoS One* **7,** e43199 CrossRef Medline
20. Panettieri, R. A., Jr, Goldie, R. G., Rigby, P. J., Eszterhas, A. J., and Hay, D. W. (1996) Endothelin-1-induced potentiation of human airway smooth muscle proliferation: an ETA receptor-mediated phenomenon. *Br. J. Pharmacol.* **118,** 191–197 CrossRef Medline
21. Walsh, K. P., Minamide, L. S., Kane, S. J., Shaw, A. E., Brown, D. R., Pulford, B., Zabel, M. D., Lambeth, J. D., Kuhn, T. B., and Bamburg, J. R. (2014) Amyloid-β and proinflammatory cytokines utilize a prion protein-dependent pathway to activate NADPH oxidase and induce cofilin-actin rods in hippocampal neurons. *PLoS One* **9,** e95995 CrossRef Medline
22. Minamide, L. S., Striegl, A. M., Boyle, J. A., Meberg, P. J., and Bamburg, J. R. (2000) Neurodegenerative stimuli induce persistent ADF/cofilin-actin rods that disrupt distal neurite function. *Nat. Cell Biol.* **2,** 628–636 CrossRef Medline
23. Altenhöfer, S., Kleikers, P. W., Radermacher, K. A., Scheurer, P., Rob Hermans, J. J., Schiffers, P., Ho, H., Wingler, K., and Schmidt, H. H. (2012) The NOX toolbox: validating the role of NADPH oxidases in physiology and disease. *Cell. Mol. Life Sci.* **69,** 2327–2343 CrossRef Medline
24. De La Cruz, E. M. (2009) How cofilin severs an actin filament. *Biophys. Rev.* **1,** 51–59 CrossRef Medline
25. Wang, Y., Shibasaki, F., and Mizuno, K. (2005) Calcium signal-induced cofilin dephosphorylation is mediated by Slingshot via calcineurin. *J. Biol. Chem.* **280,** 12683–12689 CrossRef Medline
26. Niwa, R., Nagata-Ohashi, K., Takeichi, M., Mizuno, K., and Uemura, T. (2002) Control of actin reorganization by Slingshot, a family of phosphatases that dephosphorylate ADF/cofilin. *Cell* **108,** 233–246 CrossRef Medline
27. Scott, R. W., Hooper, S., Crighton, D., Li, A., König, I., Munro, J., Trivier, E., Wickman, G., Morin, P., Croft, D. R., Dawson, J., Machesky, L., Anderson, K. I., Sahai, E. A., and Olson, M. F. (2010) LIM kinases are required for invasive path generation by tumor and tumor-associated stromal cells. *J. Cell Biol.* **191,** 169–185 CrossRef Medline
28. Grimm, A., Cummins, N., and Götz, J. (2018) Local oxidative damage in the soma and dendrites quarantines neuronal mitochondria at the site of insult. *iScience* **6,** 114–127 CrossRef Medline
29. Lin, Y. C., and Koleske, A. J. (2010) Mechanisms of synapse and dendrite maintenance and their disruption in psychiatric and neurodegenerative disorders. *Annu. Rev. Neurosci.* **33,** 349–378 CrossRef Medline
30. Rust, M. B., Gurniak, C. B., Renner, M., Vara, H., Morando, L., Görlich, A., Sassoè-Pognetto, M., Banchaabouchi, M. A., Giustetto, M., Triller, A., Choquet, D., and Witke, W. (2010) Learning, AMPA receptor mobility and synaptic plasticity depend on n-cofilin-mediated actin dynamics. *EMBO J.* **29,** 1889–1902 CrossRef Medline
31. Pontrello, C. G., Sun, M. Y., Lin, A., Fiacco, T. A., DeFea, K. A., and Ethell, I. M. (2012) Cofilin under control of β-arrestin-2 in NMDA-dependent dendritic spine plasticity, long-term depression (LTD), and learning. *Proc. Natl. Acad. Sci. U.S.A.* **109,** E442–E451 CrossRef Medline
32. Woo, J. A., Zhao, X., Khan, H., Penn, C., Wang, X., Joly-Amado, A., Weeber, E., Morgan, D., and Kang, D. E. (2015) Slingshot-Cofilin activation mediates mitochondrial and synaptic dysfunction via Aβ ligation to β1-integrin conformers. *Cell Death Differ.* **22,** 921–934 CrossRef Medline
33. Briyal, S., Philip, T., and Gulati, A. (2011) Endothelin-A receptor antagonists prevent amyloid-β-induced increase in ETA receptor expression, oxidative stress, and cognitive impairment. *J. Alzheimers Dis.* **23,** 491–503 CrossRef Medline
34. Lo, A. C., Chen, A. Y., Hung, V. K., Yaw, L. P., Fung, M. K., Ho, M. C., Tsang, M. C., Chung, S. S., and Chung, S. K. (2005) Endothelin-1 overexpression leads to further water accumulation and brain edema after middle cerebral artery occlusion via aquaporin 4 expression in astrocytic endfeet. *J. Cereb. Blood Flow Metab.* **25,** 998–1011 CrossRef Medline
35. Loomis, E. D., Sullivan, J. C., Osmond, D. A., Pollock, D. M., and Pollock, J. S. (2005) Endothelin mediates superoxide production and vasoconstriction through activation of NADPH oxidase and uncoupled nitric-oxide synthase in the rat aorta. *J. Pharmacol. Exp. Ther.* **315,** 1058–1064 CrossRef Medline
36. Briyal, S., Nguyen, C., Leonard, M., and Gulati, A. (2015) Stimulation of endothelin B receptors by IRL-1620 decreases the progression of Alzheimer's disease. *Neuroscience* **301,** 1–11 CrossRef Medline
37. Briyal, S., Shepard, C., and Gulati, A. (2014) Endothelin receptor type B agonist, IRL-1620, prevents β amyloid (Aβ) induced oxidative stress and cognitive impairment in normal and diabetic rats. *Pharmacol. Biochem. Behav.* **120,** 65–72 CrossRef Medline
38. Li, J. J., Wu, L. H., Cao, Q., Yuan, Y., Yang, L., Guo, Z. Y., Kaur, C., Sivakumar, V., Ling, E. A., and Wu, C. Y. (2010) Endothelins-1/3 and endothelin-A/B receptors expressing glial cells with special reference to activated microglia in experimentally induced cerebral ischemia in the adult rats. *Neuroscience* **167,** 665–677 CrossRef Medline
39. Wilkinson, B. L., and Landreth, G. E. (2006) The microglial NADPH oxidase complex as a source of oxidative stress in Alzheimer's disease. *J. Neuroinflammation* **3,** 30 CrossRef Medline
40. Koizumi, K., Wang, G., and Park, L. (2016) Endothelial dysfunction and amyloid-β-induced neurovascular alterations. *Cell. Mol. Neurobiol.* **36,** 155–165 CrossRef Medline
41. Abramov, A. Y., Canevari, L., and Duchen, M. R. (2004) β-Amyloid peptides induce mitochondrial dysfunction and oxidative stress in astrocytes and death of neurons through activation of NADPH oxidase. *J. Neurosci.* **24,** 565–575 CrossRef Medline
42. Kaech, S., and Banker, G. (2006) Culturing hippocampal neurons. *Nat. Protoc.* **1,** 2406–2415 CrossRef Medline
43. Hung, K. L. V. (2008) *The Role of Astrocytic Endothelin-1 in Dementia Associated with Alzheimer's Disease and Mild Ischemic Stroke*. Ph.D. thesis, The University of Hong Kong CrossRef

Endothelin type B receptor promotes cofilin rod formation and dendritic loss in neurons by inducing oxidative stress and cofilin activation

Sze-Wah Tam, Rui Feng, Way Kwok-Wai Lau, Andrew Chi-Kin Law, Patrick Ka-Kit Yeung and Sookja Kim Chung

J. Biol. Chem. 2019, 294:12495-12506.
doi: 10.1074/jbc.RA118.005155 originally published online June 27, 2019